JOC Article
pubs.acs.org/joc

Computational Studies of Ion-Pair Separation of Benzylic Organolithium Compounds in THF: Importance of Explicit and Implicit Solvation

Nipa Deora and Paul R. Carlier*

Department of Chemistry, Virginia Tech, Blacksburg, Virginia 24060

pcarlier@vt.edu

Received July 31, 2009

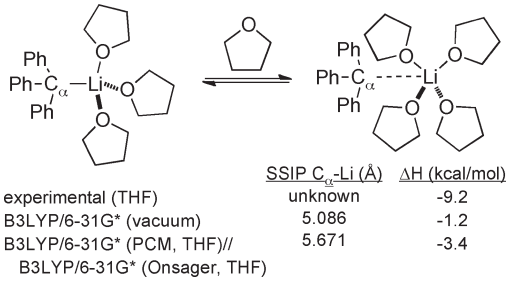

Ion-pair separation (IPS) of THF-solvated fluorenyl ($\mathbf{1_C}$), diphenylmethyl ($\mathbf{2_C}$), and trityl ($\mathbf{3_C}$) lithium was studied computationally. Minimum energy equilibrium geometries of explicit bis- and tris-solvated contact ion pairs (CIPs) and tetrakis-solvated separated ion pairs (SIPs) were located at B3LYP/6-31G*. Associative transition structures linking the tris-solvated CIPs and tetrakis-solvated SIPs were also located. Based on MP2/6-31G*//B3LYP/6-31G* energies, the resting states of the CIPs are predicted to be trisolvates. Calculated enthalpies of IPS (ΔH_{IPS}) at 298 K were compared to experimental (UV−vis spectroscopy) solution values reported in the literature. In vacuum, B3LYP/6-31G* ΔH_{IPS} values for $\mathbf{1_C}\cdot(THF)_3$−$\mathbf{3_C}\cdot(THF)_3$ are 6−8 kcal/mol less exothermic than the experimentally determined values in THF solution. Closer examination of the individual steps of ion-pair separation (ionization, solvation, ion-pair recombination), as well as comparison of calculated structures with the published X-ray structures of $\mathbf{1_C}\cdot(THF)_3$ and $\mathbf{3_S}\cdot(THF)_4$, suggested that in vacuo modeling of the SSIPs was problematic. Incorporation of secondary solvation in the form of Onsager and PCM single-point calculations showed an increase in exothermicity of IPS. Application of a continuum solvation model (Onsager) during optimization at the B3LYP/6-31G* level of theory produced significant changes in the C_α−Li contact distances in the SSIPs, and B3LYP/6-31G* (PCM)//B3LYP/6-31G* (Onsager) energies bring ΔH_{IPS} within 5−6 kcal/mol of experiment. Possible strategies to achieve closer agreement with experiment are discussed.

Introduction

The role of organolithium chemistry in asymmetric synthesis is well-known,[1] and enantioenriched configurationally stable organolithium intermediates feature in numerous reactions.[2−8] Racemization of the key intermediates in these reactions can occur via a number of mechanisms, including the conducted tour mechanism,[9,10] by a radical pathway (SET mechanism),[3,11]

*Corresponding author. Fax: (540) 231-3255.

(1) Luderer, M. R.; Bailey, W. F.; Luderer, M. R.; Fair, J. D.; Dancer, R. J.; Sommer, M. B. *Tetrahedron: Asymmetry* **2009**, *20*, 981–998.
(2) Basu, A.; Thayumanavan, S. *Angew. Chem., Int. Ed.* **2002**, *41*, 716–738.
(3) Gawley, R. E. *J. Org. Chem.* **2006**, *71*, 2411–2416.
(4) Clayden, J.; Dufour, J.; Grainger, D. M.; Helliwell, M. *J. Am. Chem. Soc.* **2007**, *129*, 7488–7489.
(5) Clayden, J.; Hennecke, U. *Org. Lett.* **2008**, *10*, 3567–3570.
(6) Coldham, I.; Patel, J. J.; Raimbault, S.; Whittaker, D. T. E.; Adams, H.; Fang, G. Y.; Aggarwal, V. K. *Org. Lett.* **2008**, *10*, 141–143.
(7) Sonawane, R. P.; Muck-Lichtenfeld, C.; Frohlich, R.; Bergander, K.; Hoppe, D. *Chem.—Eur. J.* **2007**, *13*, 6419–6429.
(8) Kapeller, D. C.; Brecker, L.; Hammerschmidt, F. *Chem.—Eur. J.* **2007**, *13*, 9582–9588.
(9) Clayden, J.; Stimson, C. C.; Keenan, M.; Wheatley, A. E. H. *Chem. Commun.* **2004**, 228–229.
(10) Low, E.; Gawley, R. E. *J. Am. Chem. Soc.* **2000**, *122*, 9562–9563.
(11) Juaristi, E.; Jimenezvazquez, H. A. *J. Org. Chem.* **1991**, *56*, 1623–1630.
(12) Peoples, P. R.; Grutzner, J. B. *J. Am. Chem. Soc.* **1980**, *102*, 4709–4715.

DOI: 10.1021/jo9016452 Published on Web 01/27/2010

or by ion-pair separation (IPS).[12] In ethereal solvents, this latter process is thought to occur by association of the solvated contact ion pair (CIP) with an additional solvent molecule, giving a solvent-separated ion pair (SSIP). We have previously studied racemization of lithiated cyclopropyl nitriles by a conducted tour mechanism.[13] As a prelude to a computational study of racemization by an IPS mechanism, we sought to determine whether modern computational methods could adequately model the thermodynamics of IPS. In addition, these studies could also be useful for predicting the ionization state of highly stabilized organolithiums. Extensive experimental work relating the ionization state of organolithium compounds to reactivity has been carried out by Reich and co-workers.[14−16] SSIPs can be less[16] or more[16−18] reactive than the corresponding CIPs, and this difference in reactivity can lead to changes in the course of reactions.[14,15,19−21] Ionizability of alkyllithiums also plays a significant role in anionic polymerization reactions, wherein the dissociated carbanion is the main propagating species, upon which the rate of polymerization depends.[22] A validated computational approach to assess IPS could thus prove useful for prediction of the outcome of organolithium reactions.

Numerous theoretical studies of organolithium contact ion pairs in ethereal solvents have addressed solvation number and aggregation states.[23−27] To the best of our knowledge, only one theoretical study addressing organolithium ion-pair separation has been reported in the literature. Müller et al. studied the conversion of tris-THF-solvated 1-lithioethylbenzene to the corresponding tetrakis-THF-solvated separated ion pair.[28] The energies of IPS (ΔE_{IPS}, B3P86/SVP and B3LYP/TZVP//B3P86/SVP) were calculated to be +4.4 and +5.9 kcal/mol, respectively. Yet because no experimental data has been reported for this system, it has not been possible to assess the accuracy of these estimates.

SCHEME 1. Experimental Enthalpies (ΔH_{IPS}) for Ion-Pair Separation (kcal/mol) of Fluorenyllithium ($\mathbf{1_C}$), Diphenylmethyllithium ($\mathbf{2_C}$), and Trityllithium ($\mathbf{3_C}$) in THF Solution, As Determined by UV−vis Spectroscopy[a]

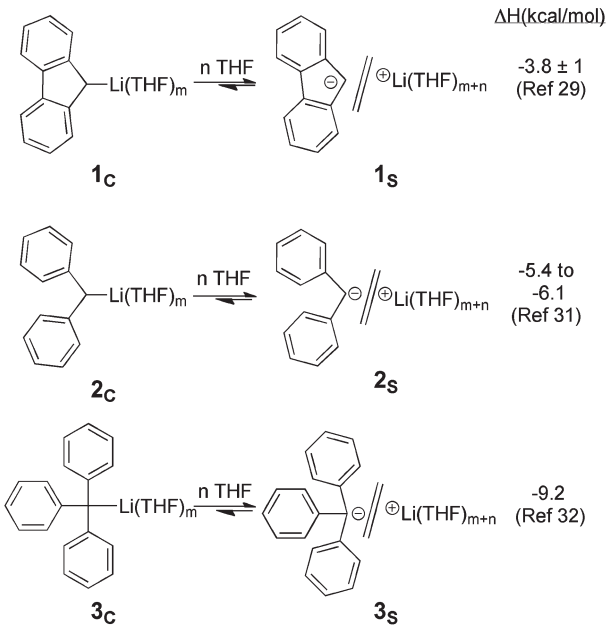

[a]Values of *m* and *n* in each case are not known from experiment.

Experimental data is, however, available for the IPS themodynamics of other benzylic organolithium systems, including fluorenyl (Fl),[29,30] diphenylmethyl (DPM),[31] and triphenylmethyl (Tr)[32] lithium compounds. Hogen-Esch and Smid used UV−vis spectroscopy to study the effects of temperature, counterion, and solvent on ion-pair separation of various fluorenyl metal salts in ethereal solvents.[33] The value of ΔH_{IPS} for Fl−Li CIP $\mathbf{1_C}$ in THF was found to be approximately −7.0 kcal/mol; however, the authors cautioned that this value might be inaccurate due to the high degree of dissociation to SSIP at room temperature. Subsequent ^{13}C NMR studies of Fl−Li **1** in THF by O'Brien gave $\Delta H_{IPS} = -4.9 \pm 1$ kcal/mol.[30,34] The most recent, and in our opinion, most reliable determination of ΔH_{IPS} of $\mathbf{1_C}$ in THF stems from Streitwieser's UV−vis spectroscopic study (263−328 K), which gave $\Delta H_{IPS} = -3.8 \pm 1$ kcal/mol (Scheme 1).[29]

UV−vis spectroscopic studies of the IPS of DPM−Li **2** (215−296 K)[31] and Tr−Li **3** (263 to 328K)[32] in THF were reported by Buncel. IPS was found to be exothermic in both cases, with ΔH_{IPS} of −5.4 to −6.1 kcal/mol for DPM−Li $\mathbf{2_C}$ and −9.2 kcal/mol for Tr−Li $\mathbf{3_C}$. Therefore, the UV−vis spectroscopic studies of Streitwieser and Buncel indicate that IPS of $\mathbf{3_C}$ is the most exothermic in the series by 4−5 kcal/mol and that $\mathbf{2_C}$ and $\mathbf{1_C}$ have similar values of ΔH_{IPS} (Scheme 1). In this paper, we will assess to what degree modern computational

(13) Carlier, P. R. *Chirality* **2003**, *15*, 340–347.
(14) Reich, H. J.; Holladay, J. E.; Mason, J. D.; Sikorski, W. H. *J. Am. Chem. Soc.* **1995**, *117*, 12137–12150.
(15) Reich, H. J.; Sikorski, W. H. *J. Org. Chem.* **1999**, *64*, 14–15.
(16) Reich, H. J.; Sanders, A. W.; Fiedler, A. T.; Bevan, M. J. *J. Am. Chem. Soc.* **2002**, *124*, 13386–13387.
(17) Ellington, J. C.; Arnett, E. M. *J. Am. Chem. Soc.* **1988**, *110*, 7778–7785.
(18) Krom, J. A.; Streitwieser, A. *J. Am. Chem. Soc.* **1992**, *114*, 8747–8748.
(19) Sikorski, W. H.; Reich, H. J. *J. Am. Chem. Soc.* **2001**, *123*, 6527–6535.
(20) Canepa, C.; Prandi, C.; Venturello, P. *Tetrahedron* **1994**, *50*, 8161–8168.
(21) Cohen, T.; Abraham, W. D.; Myers, M. *J. Am. Chem. Soc.* **1987**, *109*, 7923–7924.
(22) Szwarc, M. *Proc. R. Soc. London, Ser. A, Math. Phys. Sci.* **1964**, *279*, 260–290.
(23) Abbotto, A.; Streitwieser, A.; Schleyer, P. v. R. *J. Am. Chem. Soc.* **1997**, *119*, 11255–11268.
(24) Pratt, L. M.; Mogali, S.; Glinton, K. *J. Org. Chem.* **2003**, *68*, 6484–6488.
(25) Pratt, L. M.; Nguyen, S. C.; Thanh, B. T. *J. Org. Chem.* **2008**, *73*, 6086–6091.
(26) Streitwieser, A. *J. Mol. Model.* **2006**, *12*, 673–680.
(27) Pratt, L. M. *THEOCHEM* **2007**, *811*, 191–196.
(28) Yakimansky, A. V.; Müller, A. H. E.; Van Beylen, M. *Macromolecules* **2000**, *33*, 5686–5692.
(29) Gronert, S.; Streitwieser, A. *J. Am. Chem. Soc.* **1988**, *110*, 2836–2842.
(30) O'Brien, D. H.; Russell, C. R.; Hart, A. J. *J. Am. Chem. Soc.* **1979**, *101*, 633–639.
(31) Buncel, E.; Menon, B. C.; Colpa, J. P. *Can. J. Chem.* **1979**, *57*, 999–1005.
(32) Buncel, E.; Menon, B. *J. Org. Chem.* **1979**, *44*, 317–320.
(33) Hogen-Esch, T. E.; Smid, J. *J. Am. Chem. Soc.* **1966**, *88*, 307–318.
(34) O'Brien and coworkers also studied ion pair separation of Fl−Li, DPM−Li, and Tr−Li in 2-methyltetrahydrofuran; exothermicities were slightly greater. (O' Brien, D. H.; Russell, C. R.; Hart, A. J. *J. Am. Chem. Soc.* **1979**, *101*, 633−639). However, since modeling solvates of a racemic solvent would add considerable complexity, we do not include these data in this study.

methods can reproduce these experimental solution phase ΔH_{IPS} values. In particular, we will address the role of both explicit and implicit solvation in correctly modeling the structures of contact and separated ion pairs and how these solvation models influence the calculated enthalpies of ion-pair separation.

Computational Methods

All calculations were performed using Gaussian 03.[35] The B3LYP/6-31G* method and basis were chosen for all geometry optimizations to compromise between accuracy and computational economy for the large explicit solvates described in this study (e.g., 84 atoms for $\mathbf{3_S}\cdot(THF)_4$, corresponding to 694 basis functions at 6-31G*). All B3LYP/6-31G* stationary points were characterized by vibrational frequency analysis as minima (zero imaginary frequencies) or transition structures (one imaginary frequency). Although molecular dynamics may ultimately provide the best method to determine average equilibrium solvation numbers,[36,37] a number of recent studies have modeled the thermodynamics of ethereal solvation of organolithiums by locating explicit solvates.[38−41] These and related studies have revealed that Me_2O is not a reliable surrogate for THF[25,40,41] and have noted the practical impossibility of exhaustively sampling the large conformational space available to THF-solvated organolithiums.[40,42] To address this latter concern, multiple initial geometries of the explicit solvates were sequentially constructed and optimized to ensure uniform sampling of the conformational space available to the $Li(THF)_n$ fragments in the fluorenyl, diphenylmethyl, and trityl series ($n = 2-4$). Further details on this iterative optimization procedure are given below and in the Supporting Information. Frequencies were scaled with the B3LYP/6-31G* ZPVE correction factor of 0.9815 to calculate enthalpic corrections at 298 K.[43]

Although we would always prefer to benchmark density functional calculations against post-Hartree−Fock methods,[44] molecular size considerations rendered MP2 optimizations impractical. Thus, MP2/6-31G* single-point calculations were performed on B3LYP/6-31G*-optimized geometries. To explore basis set size effects, select B3LYP single-point calculations were performed with the 6-31+G* basis set. Select mPW1PW91/6-31G* single-point calculations were also performed to assess the effect of another density functional on the thermodynamics of IPS.

To model bulk solvent effects, continuum solvation models were applied in two ways. First, implicit solvation (THF, $\varepsilon = 7.58$) was modeled by means of Onsager and PCM single-point calculations on the B3LYP/6-31G* (vacuum) geometries; these dual-level calculations are denoted as B3LYP/6-31G* (Onsager)//B3LYP/6-31G* and B3LYP/6-31G* (PCM)//B3LYP/6-31G*. Van Speybroeck and co-workers have recently used the single-point correction approach to model bulk solvent effects on explicitly solvated lithiated α-aminophosphonates[45] and lithiated imines.[46] Onsager single-point calculations require specification of a radius (a_0). Since the Volume keyword of Gaussian '03 invokes a Monte Carlo integration method to determine this parameter, a_0 is *not* uniquely determined by the geometry. Uncertainty in a_0 will propagate into uncertainty in energy and uncertainty in ΔH_{IPS}. In 10 identical repeat volume calculations of $\mathbf{1_C}\cdot(THF)_3$, a standard deviation of 3.7% (0.22 Å) was seen in radius a_0. This random error must be considered but may not sufficiently address systematic error stemming from the use of a spherical cavity to contain nonspherical molecules. Therefore, to provide a conservative estimate of the uncertainty in Onsager energy for all the calculated species in the paper, we allowed a_0 to vary by ±10%. Thus, for every species in the paper a specific radius a_0 was determined by a single Volume calculation on the vacuum-optimized geometry, and Onsager single-point electronic energies were performed at radii of a_0, $0.9a_0$, and $1.1a_0$. The mean Onsager energies and their standard deviations were then determined. Since uncertainty in ΔH_{IPS} derives only from uncertainties in the energies, a standard formula for propagation of errors in a sum of terms was applied: $\sigma_{\Delta H(IPS)} \approx \sigma_{\Delta E(IPS)} = (\sigma_{E(SSIP)}{}^2 + \sigma_{E(CIP)}{}^2 + \sigma_{E(THF)}{}^2)^{0.5}$. These uncertainties in Onsager energy-based values of ΔH_{IPS} are reported in Table 4. PCM single-point calculations were performed with the options surface = SES and radii = pauling; Pauling radii have been recommended for ionic species.[46]

To incorporate the effect of a dielectric *during geometry optimization*, we used the Onsager continuum model. The a_0 values determined for the vacuum geometries were used as input in these optimizations, which we denote as B3LYP/6-31G* (Onsager). As described above, single-point Onsager energies on these geometries were determined at $0.9a_0$ and $1.1a_0$ to assess the uncertainty in ΔH_{IPS}. Note that geometry optimization of the large solvated CIPs and SSIPs under PCM solvation was attempted but proved unsuccessful. Finally, basis set superposition error was estimated by performing counterpoise calculations on the B3LYP/6-31G* and B3LYP/6-31G* (Onsager) geometries of the tetrakis(THF)-solvated separated ion pairs ($\mathbf{1_S}\cdot(THF)_4-\mathbf{3_S}\cdot(THF)_4$). For each structure, multiple counterpoise corrections were performed by sequentially designating each of the bound THF molecules as the secondary fragment. These individual corrections were then averaged to give the counterpoise correction for a particular structure.

Modeling of Explicitly Solvated Contact and Separated Ion Pairs. Before the thermodynamics of ion-pair separation of $\mathbf{1_C}-\mathbf{3_C}$ can be addressed computationally, the resting THF solvation number of these species and of the corresponding

(35) *Gaussian 03, Revision B.05*: Frisch, M. J.; Trucks, G. W.; Schlegel, H. B.; Scuseria, G. E.; Robb, M. A.; Cheeseman, J. R.; Montgomery, J. A., Jr.; Vreven, T.; Kudin, K. N.; Burant, J. C.; Millam, J. M.; Iyengar, S. S.; Tomasi, J.; Barone, V.; Mennucci, B.; Cossi, M.; Scalmani, G.; Rega, N.; Petersson, G. A.; Nakatsuji, H.; Hada, M.; Ehara, M.; Toyota, K.; Fukuda, R.; Hasegawa, J.; Ishida, M.; Nakajima, T.; Honda, Y.; Kitao, O.; Nakai, H.; Klene, M.; Li, X.; Knox, J. E.; Hratchian, H. P.; Cross, J. B.; Adamo, C.; Jaramillo, J.; Gomperts, R.; Stratmann, R. E.; Yazyev, O.; Austin, A. J.; Cammi, R.; Pomelli, C.; Ochterski, J. W.; Ayala, P. Y.; Morokuma, K.; Voth, G. A.; Salvador, P.; Dannenberg, J. J.; Zakrzewski, V. G.; Dapprich, S.; Daniels, A. D.; Strain, M. C.; Farkas, O.; Malick, D. K.; Rabuck, A. D.; Raghavachari, K.; Foresman, J. B.; Ortiz, J. V.; Cui, Q.; Baboul, A. G.; Clifford, S.; Cioslowski, J.; Stefanov, B. B.; Liu, G.; Liashenko, A.; Piskorz, P.; Komaromi, I.; Martin, R. L.; Fox, D. J.; Keith, T.; Al-Laham, M. A.; Peng, C. Y.; Nanayakkara, A.; Challacombe, M.; Gill, P. M. W.; Johnson, B.; Chen, W.; Wong, M. W.; Gonzalez, C.; Pople, J. A. Gaussian, Inc.: Pittsburgh, PA, 2003.

(36) Gérard, H.; de la Lande, A.; Maddalunu, J.; Parisel, O.; Tuckerman, M. E. *J. Phys. Chem. A* **2006**, *110*, 4787–4794.

(37) Declerck, R.; De Sterck, B.; Verstraelen, T.; Verniest, G.; Mangelinckx, S.; Jacobs, J.; De Kimpe, N.; Waroquier, M.; Van Speybroeck, V. *Chem.—Eur. J.* **2009**, *15*, 580–584.

(38) Pratt, L. M.; Ramachandran, B.; Xidos, J. D.; Cramer, C. J.; Truhlar, D. G. *J. Org. Chem.* **2002**, *67*, 7607–7612.

(39) Pratt, L. M.; Truhlar, D. G.; Cramer, C. J.; Kass, S. R.; Thompson, J. D.; Xidos, J. D. *J. Org. Chem.* **2007**, *72*, 2962–2966.

(40) Pratt, L. M.; Jones, D.; Sease, A.; Busch, D.; Faluade, E.; Nguyen, S. C.; Thanh, B. T. *Int. J. Quantum Chem.* **2009**, *109*, 34–42.

(41) Dixon, D. D.; Tius, M. A.; Pratt, L. M. *J. Org. Chem.* **2009**, *74*, 5881–5886.

(42) Khartabil, H. K.; Gros, P. C.; Fort, Y.; Ruiz-López, M. F. *J. Org. Chem.* **2008**, *73*, 9393–9402.

(43) Merrick, J. P.; Moran, D.; Radom, L. *J. Phys. Chem. A* **2007**, *111*, 11683–11700.

(44) Carlier, P. R.; Deora, N.; Crawford, T. D. *J. Org. Chem.* **2006**, *71*, 1592–1597.

(45) Van Speybroeck, V.; Moonen, K.; Hemelsoet, K.; Stevens, C. V.; Waroquier, M. *J. Am. Chem. Soc.* **2006**, *128*, 8468–8478.

(46) De Sterck, B.; Van Speybroeck, V.; Mangelinckx, S.; Verniest, G.; De Kimpe, N.; Waroquier, M. *J. Phys. Chem. A* **2009**, *113*, 6375–6380.

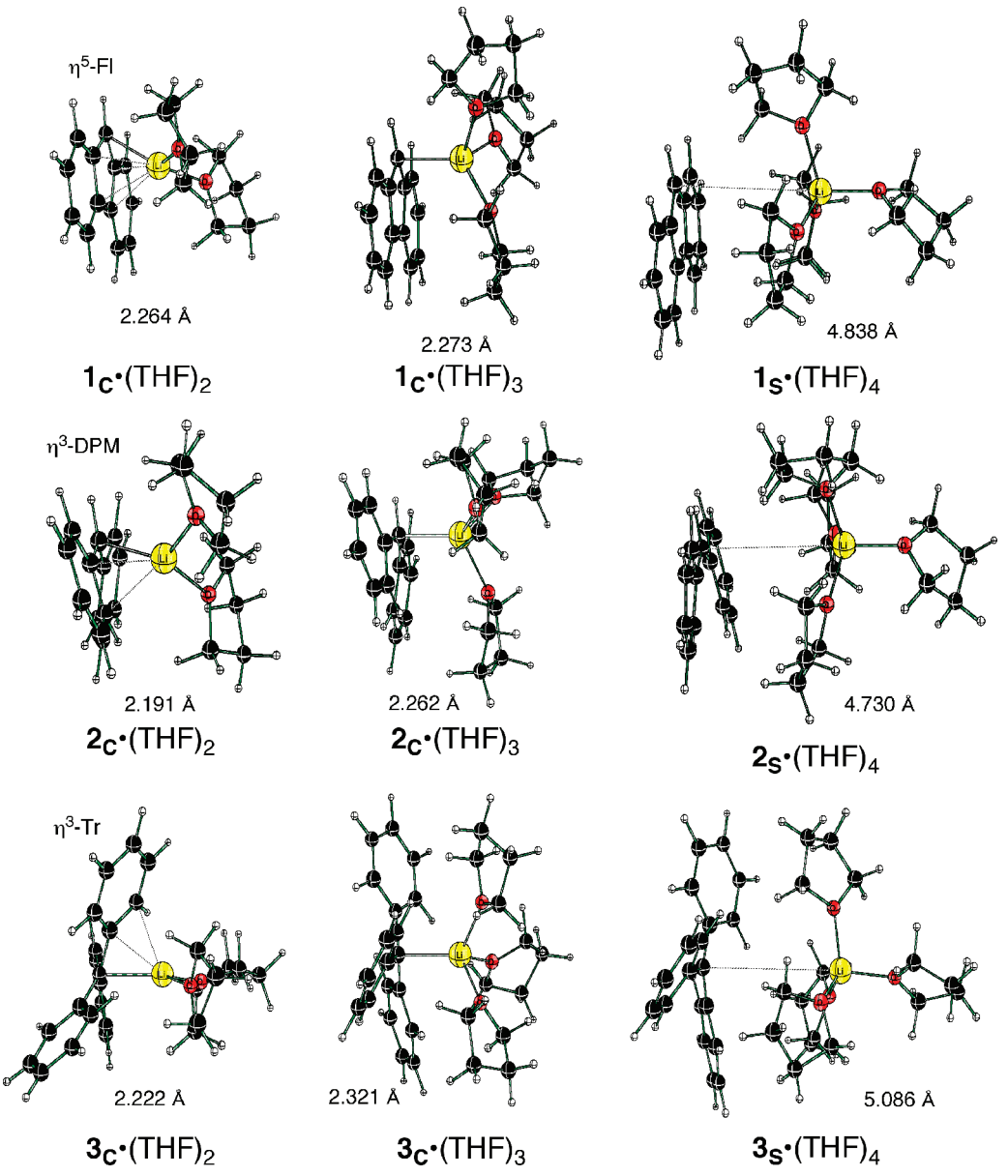

FIGURE 1. Minimum energy B3LYP/6-31G* equilibrium geometries of bis-THF solvated contact ion pairs $\mathbf{1_C}\cdot(THF)_2$–$\mathbf{3_C}\cdot(THF)_2$, tris-THF solvated contact ion pairs $\mathbf{1_C}\cdot(THF)_3$–$\mathbf{3_C}\cdot(THF)_3$, and tetrakis-THF-solvated separated ion pairs $\mathbf{1_S}\cdot(THF)_4$–$\mathbf{3_S}\cdot(THF)_4$; C_α–Li distances are shown in each case.

separated ion pairs $\mathbf{1_S}$–$\mathbf{3_S}$ must be established. Because these values have not been determined experimentally in solution, we examined ethereal solvates of **1**–**3** that have been characterized by X-ray crystallography. Fluorenyllithium **1** has been characterized as the tris(THF)-solvated CIP ($\mathbf{1_C}\cdot(THF)_3$),[47] as the bis(Et_2O)-solvated CIP ($\mathbf{1_C}\cdot(Et_2O)_2$; note: η^2-fluorenyl),[48] and as a bis(diglyme)-solvated SIP ($\mathbf{1_S}\cdot(\eta^3\text{-diglyme})_2$)[49] With regard to DPM-Li **2**, only a bis(12-crown-4)-solvated SIP ($\mathbf{2_S}\cdot(\eta^4\text{-12-crown-4})_2$)[50] has been characterized by X-ray crystallography. Finally, TrLi **3** has been characterized in the solid state as a bis(Et_2O)-solvated CIP ($\mathbf{3_C}\cdot(Et_2O)_2$; note: η^3-trityl),[51] a tetrakis(THF)-solvated SIP ($\mathbf{3_C}\cdot(THF)_4$),[52] and a bis(12-crown-4)-solvated SIP ($\mathbf{3_S}\cdot(\eta^4\text{-12-crown-4})_2$).[50]

Given that $\mathbf{1_C}$ has been characterized in the solid state as both bis(Et_2O) and tris(THF) solvates, we applied computational methods to address the resting solvation numbers of THF-solvated $\mathbf{1_C}$–$\mathbf{3_C}$. To minimize the chance that calculated energies of bis- and tris(THF)-solvated $\mathbf{1_C}$–$\mathbf{3_C}$ were biased by different conformations of the $Li(THF)_n$ fragment, we carried out multiple sequential B3LYP/6-31G* optimizations. In this procedure the THF-solvated lithium fragments of each optimized geometry were swapped between the various carbanion fragments (Fl^-, DPM^-, Tr^-), and the resulting new initial

(47) Olbrich, F. Private communication to the Cambridge Structural Database, deposition no. CCDC 114095, 2002.
(48) Hakansson, M.; Ottosson, C. H.; Boman, A.; Johnels, D. *Organometallics* **1998**, *17*, 1208–1214.
(49) Neander, S.; Kornich, J.; Olbrich, F. *J. Organomet. Chem.* **2002**, *656*, 89–96.
(50) Olmstead, M. M.; Power, P. P. *J. Am. Chem. Soc.* **1985**, *107*, 2174–2175.
(51) Bartlett, R. A.; Dias, H. V. R.; Power, P. P. *J. Organomet. Chem.* **1988**, *341*, 1–9.
(52) Fernandez, I.; Martinez-Viviente, E.; Breher, F.; Pregosin, P. S. *Chem.—Eur. J.* **2005**, *11*, 1495–1506.

TABLE 1. Enthalpy (ΔH_{SOLV3}) and Free Energy (ΔG_{SOLV3}) and for the Third THF Solvation of Contact Ion Pairs $\mathbf{1_C}$−$\mathbf{3_C}$ (298 K, kcal/mol)[a]

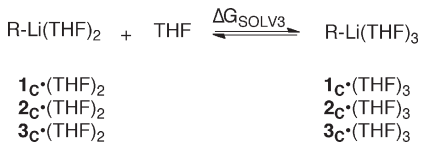

method/basis		**1** (R = Fl)	**2** (R = DPM)	**3** (R = Tr)
B3LYP/6-31G*	ΔH_{SOLV3}	−6.5	−6.7	−7.8
	ΔG_{SOLV3}	+4.8	+2.9	+5.8
MP2/6-31G*// B3LYP/6-31G*	ΔH_{SOLV3}	−12.6	−13.9	−18.7
	ΔG_{SOLV3}	−1.3	−4.4	−5.1

[a]Enthalpy $\Delta H_{SOLV3} = H(\text{R−Li(THF)}_3) - [H(\text{R−Li(THF)}_2) + (\text{THF})]$; free energy $\Delta G_{SOLV3} = G(\text{R−Li(THF)}_3) - [G(\text{R−Li(THF)}_2) + \text{G(THF)}]$; all values in kcal/mol. Free energy and enthalpy corrections (298 K) to the absolute energies were determined from B3LYP/6-31G* frequencies, scaled by 0.9815.

geometries were reoptimized. After three to four generations of optimization, no new lowest energy minima were found (see Figures S4 and S5 in the Supporting Information for details). The minimum energy equilibrium geometries of the bis(THF)-solvates and tris(THF)-solvates of $\mathbf{1_C}$−$\mathbf{3_C}$ found in this way are depicted in Figure 1.

Several features of the calculated structures of the bis- and tris(THF)-solvated CIPs are noteworthy. First, all of the bis(THF) solvates show multiple close contacts of the lithium with the carbanion fragment: fluorenyl lithium $\mathbf{1_C}\cdot(\text{THF})_2$ is η^5-coordinated, and the carbanionic fragments in $\mathbf{2_C}\cdot(\text{THF})_2$ and $\mathbf{3_C}\cdot(\text{THF})_2$ are both η^3-coordinated (Figure 1). Thus, the calculated equilibrium geometries of these bis(THF) solvates parallel the higher hapticity seen by X-ray crystallography of related bis-solvates $\mathbf{1_C}\cdot(\text{Et}_2\text{O})_2$ (η^2-fluorenyl)[48] and $\mathbf{3_C}\cdot(\text{Et}_2\text{O})_2$ (η^3-trityl).[51] In contrast, the calculated tris(THF) solvates $\mathbf{1_C}\cdot(\text{THF})_3$−$\mathbf{3_C}\cdot(\text{THF})_3$ all show η^1-coordination, as seen in the X-ray structure of $\mathbf{1_C}\cdot(\text{THF})_3$.[47] Consistent with the reduced hapticity seen in the trisolvated structures, significant increases in the C_α−Li bond length (0.07 − 0.10 Å) are seen in $\mathbf{2_C}\cdot(\text{THF})_3$ and $\mathbf{3_C}\cdot(\text{THF})_3$ relative to the disolvates (Figure 1). Furthermore, good correspondence is seen between the calculated B3LYP/6-31G* and X-ray geometries of tris(THF)-solvated CIP (η^1-fluorenyl).[47] The calculated C_α−Li bond length of 2.273 Å is within 0.014 Å of the X-ray bond length of 2.287 Å. The calculated Li−O bond lengths (1.993−2.014 Å) are within 0.079 Å of those seen by X-ray crystallography (1.914−1.956 Å). Finally, attempts were made to construct CIP species with four coordinated THF molecules. However, in every case the fourth solvent ligand dissociated from the lithium during optimization.

With the minimum energy B3LYP/6-31G* geometries of the bis- and tris(THF)-solvated CIPs in hand, we calculated the enthalpy and free energy of the third solvation of $\mathbf{1_C}$−$\mathbf{3_C}$. Because previous studies have reported that DFT underestimates the enthalpy of the third ethereal solvation of organolithiums,[40,41] as recommended we also calculated these terms based on the MP2/6-31G*//B3LYP/6-31G* single-point energies (Table 1).

Although the third solvation is exothermic for $\mathbf{1_C}$−$\mathbf{3_C}$ at both B3LYP/6-31G* and MP2/6-31G*//B3LYP/6-31G*, the latter ΔH_{SOLV3} values are significantly (6−11 kcal) more exothermic. Consequently, the third solvation of $\mathbf{1_C}$−$\mathbf{3_C}$ is *exergonic* only at MP2/6-31G*//B3LYP/6-31G*, due to the large positive $T\Delta S$ term (+9.6 to +13.6 kcal/mol). Thus, our results match those of previous workers who reported that DFT underestimates the enthalpy of the third ethereal solvation of organolithiums.[40,41] Since the MP2/6-31G*//B3LYP/6-31G*-based values of ΔG_{SOLV3} are most consistent with the observation of tris(THF)-solvate $\mathbf{1_C}\cdot(\text{THF})_3$ in the solid state,[47] we will consider the trisolvates to be the resting state CIP structures. This conclusion is strengthened by NMR studies of LiHMDS[53,54] and 2-(α-aryl-α-lithiomethylidene)-1,1,3,3-tetramethylindan[55] in THF solution, which demonstrate tris(THF)-solvated CIPs in the temperature range employed in studies of **1**−**3**. In addition, Collum's solution studies on LiHMDS demonstrate that increasing the steric bulk of the ether solvent reduces solvation number and energy.[54] In this context, the lower solvation number seen by X-ray crystallography for the diethyl ether solvate of $\mathbf{1_C}$ (i.e., $\mathbf{1_C}\cdot(\text{Et}_2\text{O})_2$[48]) relative to the THF solvate ($\mathbf{1_C}\cdot(\text{THF})_3$[47]) is easily rationalized.

We then located minimum energy B3LYP/6-31G* equilibrium geometries of the tetrakis(THF)-solvated SIPs of the fluorenyl, diphenylmethyl, and trityl systems ($\mathbf{1_S}\cdot(\text{THF})_4$−$\mathbf{3_S}\cdot(\text{THF})_4$, see Figure 1). As described above for the CIPs, these geometries were obtained by multiple sequential B3LYP/6-31G* optimizations; after four generations of this procedure no new lower energy minima were located (see Figure S6 in the Supporting Information for details). As expected, C_α−Li distances in the tetrakis(THF)-solvated SIPs $\mathbf{1_S}\cdot(\text{THF})_4$−$\mathbf{3_S}\cdot(\text{THF})_4$ were considerably longer than those in the corresponding trisolvated CIPs, ranging from 4.730 to 5.086 Å for the three systems. However, it should be pointed out that the C_α−Li distance of 5.086 Å calculated for $\mathbf{3_S}\cdot(\text{THF})_4$ in a vacuum is considerably shorter than the distance of 6.854 Å observed by X-ray crystallography.[52] The implications of this large difference in the C_α−Li distance to the proper modeling of solution structures of SSIPs will be discussed below, following our discussion of the thermodynamics of ion-pair separation in vacuo.

Modeling Enthalpies and Activation Enthalpies of Ion-Pair Separation of Explicit Solvates in Vacuo. Based on the minimum energy B3LYP/6-31G* equilibrium geometries of the tris(THF)-solvated CIPs and the tetrakis(THF)-solvated SIPS, the enthalpy of ion-pair separation (ΔH_{IPS}) was calculated (Table 2).

At B3LYP/6-31G*, the ΔH_{IPS} value of $\mathbf{3_C}$ (−1.2 kcal/mol) was found to be roughly 3 kcal/mol more exothermic than that of $\mathbf{2_C}$ and $\mathbf{1_C}$ (both at +1.9 kcal/mol). This basic pattern in ΔH_{IPS} ($\Delta H_{IPS}(\mathbf{1}) \sim \Delta H_{IPS}(\mathbf{2}) > \Delta H_{IPS}(\mathbf{3})$) is also seen in values calculated from B3LYP/6-31+G*, mPW1PW91/6-31G*, and MP2/6-31G* single point energies (Table 2). Thus, despite varying basis set size, density functional, and method all these calculations match the experimental observation that $\Delta H_{IPS}(\mathbf{3})$ is most exothermic. However, the B3LYP/6-31G* ΔH_{IPS} values for $\mathbf{1_C}\cdot(\text{THF})_3$−$\mathbf{3_C}\cdot(\text{THF})_3$ are 6−8 kcal/mol less exothermic than indicated by experiment. Furthermore, the range of calculated ΔH_{IPS} values (1.8−3.1 kcal/mol, depending on the method) is somewhat smaller than that seen in the experimental ΔH_{IPS} values (5.4 kcal/mol).

With CIPs $\mathbf{1_C}\cdot(\text{THF})_3$−$\mathbf{3_C}\cdot(\text{THF})_3$ and SSIPs $\mathbf{1_S}\cdot(\text{THF})_4$−$\mathbf{3_S}\cdot(\text{THF})_4$ characterized, we then located associative transition

(53) Lucht, B. L.; Collum, D. B. *J. Am. Chem. Soc.* **1994**, *116*, 6009–6010.
(54) Lucht, B. L.; Collum, D. B. *J. Am. Chem. Soc.* **1995**, *117*, 9863–9874.
(55) Knorr, R.; Menke, T.; Ferchland, K.; Mehlstaubl, J.; Stephenson, D. S. *J. Am. Chem. Soc.* **2008**, *130*, 14179–14188.

TABLE 2. Experimental and Calculated ΔH_{IPS} (298 K, kcal/mol)

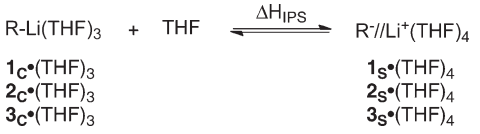

method/basis		**1** (R = Fl)	**2** (R = DPM)	**3** (R = Tr)
experimental	ΔH_{IPS}[a]	−3.8 ± 1.0[29]	−5.4 to −6.1[31]	−9.2[32]
B3LYP/6-31G*	ΔH_{IPS}[a]	+1.9	+1.9	−1.2
B3LYP/6-31+G*//B3LYP/6-31G*	ΔH_{IPS}[a]	+4.0	+4.1	+1.0
mPW1PW91/6-31G*// B3LYP/6-31G*	ΔH_{IPS}[a]	+3.6	+3.4	+0.9
MP2/6-31G*//B3LYP/6-31G*	ΔH_{IPS}[a]	+1.3	+1.9	+0.1

[a]Enthalpy value $\Delta H_{IPS} = H(SSIP) - [H(CIP) + H(THF)]$. Enthalpy corrections to absolute energies at 298 K were determined from B3LYP/6-31G* frequencies scaled by 0.9815. Experimental values determined by UV−vis spectroscopy as described in the indicated references.

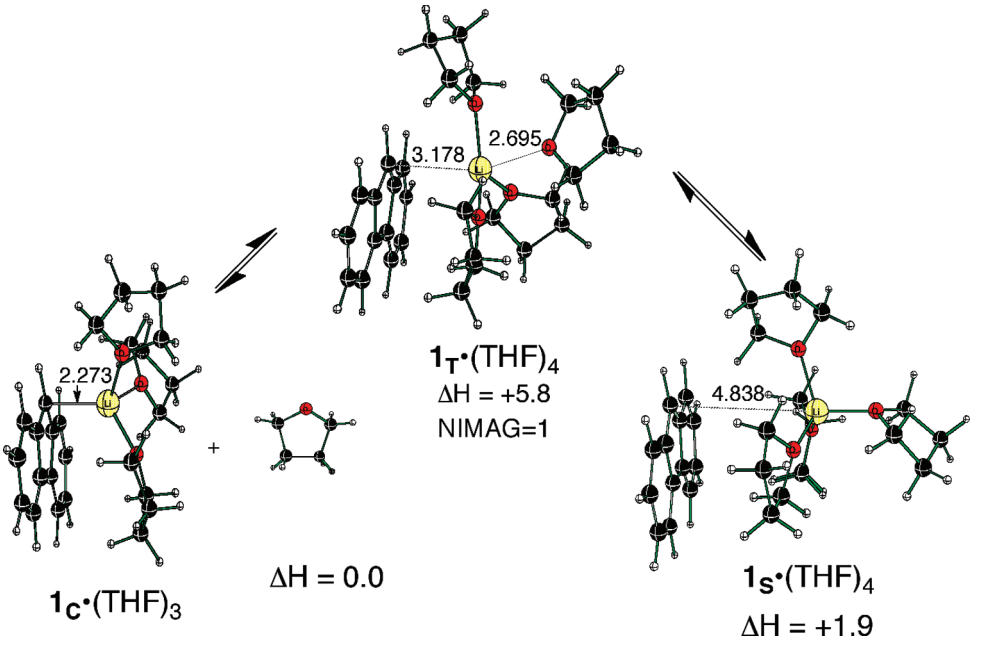

FIGURE 2. Reaction coordinate for ion-pair separation of $\mathbf{1_C}$. Enthalpies are shown in kcal/mol and are relative to the sum of $\mathbf{1_C}$ and THF. NIMAG = number of imaginary frequencies.

structures $\mathbf{1_T}\cdot(THF)_4$−$\mathbf{3_T}\cdot(THF)_4$ that interconvert these species. The reaction coordinate for $\mathbf{1_C}\cdot(THF)_3$ + THF → $\mathbf{1_T}\cdot(THF)_4$ → $\mathbf{1_S}\cdot(THF)_4$ is shown in Figure 2 (for **2** and **3** see Figures S1 and S2 in the Supporting Information). The sole imaginary frequency of each transition structure corresponds to the simultaneous breaking of the C_α−Li bond and formation of a Li−O bond due to coordination of a fourth THF ligand. An increase in C_α−Li bond distance was observed (2.273 Å in $\mathbf{1_C}\cdot(THF)_3$ to 3.178 Å in $\mathbf{1_T}\cdot(THF)_4$), and the incoming THF molecule had a considerably longer Li−O distance of 2.695 Å compared to the other three THF ligands (average O−Li 1.964 Å). The $\Delta H_{IPS}^{\ddagger}$ values range from 3.5 kcal/mol for **3**, to 5.3 kcal/mol for **2**, to 5.8 kcal/mol for IPS of **1**. These low activation barriers support the feasibility of an associative IPS mechanism. Reich and co-workers proposed an associative mechanism for IPS of bis(3,5-bistrifluoromethylphenylthio)methyllithium in THF, which also showed a relatively low barrier ($\Delta G^{\ddagger}$ = 5.3 kcal/mol).[56] Note that IPS is formally a ligand exchange on Li, and exchange of water,[57] ammonia,[57] DMSO,[58] and acetonitrile[59] have been studied computationally.[57]−59 An associative mechanism was found to be feasible in all cases.[60] However, to the best of our knowledge, $\mathbf{1_T}\cdot(THF)_4$−$\mathbf{3_T}\cdot(THF)_4$ are the first transition structures for IPS of organolithium compounds to be characterized computationally.

As discussed earlier, our calculated ΔH_{IPS} values in vacuo deviate from experimental solution values in overall exothermicity and range (Table 2). Another interesting finding is that whereas application of MP2/6-31G* single-point energies rendered the third solvation of CIPs $\mathbf{1_C}$−$\mathbf{3_C}$ 6−11 kcal/mol more exothermic than predicted at B3LYP/6-31G* (Table 1, ΔH_{solv3}), values of ΔH_{IPS} at B3LYP/6-31G* and MP2/6-31G*//B3LYP/6-31G* lie within 1.3 kcal/mol of each other (Table 2). These observations prompted us to further investigate the ion-pair separation process by isolating the key bond-breaking, -making, and ionic association steps (Figure 3).

(56) Reich, H. J.; Sikorski, W. H.; Thompson, J. L.; Sanders, A. W.; Jones, A. C. *Org. Lett.* **2006**, *8*, 4003–4006.
(57) Puchta, R.; Galle, M.; Hommes, N. V.; Pasgreta, E.; van Eldik, R. *Inorg. Chem.* **2004**, *43*, 8227–8229.
(58) Pasgreta, E.; Puchta, R.; Galle, M.; Hommes, N. V.; Zahl, A.; van Eldik, R. *ChemPhysChem* **2007**, *8*, 1315–1320.
(59) Pasgreta, E.; Puchta, R.; Zahl, A.; Van Eldik, R. *Eur. J. Inorg. Chem.* **2007**, 1815–1822.
(60) Note that in the case of exchange of water and ammonia (ref 57), Eldik and co-workers located a 5-coordinate Li minima on the potential energy surface; we found no such structures in our studies.

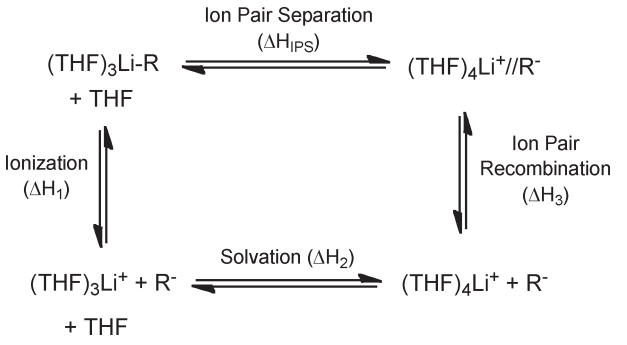

FIGURE 3. Thermodynamic cycle for ion-pair separation of THF-solvated organolithiums.

TABLE 3. Calculated ΔH_1, ΔH_2, ΔH_3, and ΔH_{IPS} for $\mathbf{1_C}\cdot(THF)_3$–$\mathbf{3_C}\cdot(THF)_3$ in kcal/mol at B3LYP/6-31G* and MP2/6-31G*//B3LYP/6-31G* (Values in Parentheses)[a]

	1 (R = Fl)	**2** (R = DPM)	**3** (R = Tr)
ΔH_1[b]	+82.5 (+100.7)	+81.2 (+100.6)	+74.7 (+98.7)
ΔH_2[c]	−16.3 (−22.8)	−16.3 (−22.8)	−16.3 (−22.8)
ΔH_3[d]	−64.2 (−76.6)	−62.9 (−75.8)	−59.5 (−75.8)
ΔH_{IPS}[e]	+1.9 (+1.3)	+1.9 (+1.9)	−1.2 (+0.1)

[a]See Figure 3 for graphical representations of ΔH_1, ΔH_2, and ΔH_3. Enthalpic corrections to absolute energies determined from B3LYP/6-31G* frequencies scaled by 0.9815. [b]$\Delta H_1 = [H(R^-) + H((THF)_3Li^+)] - H(CIP)$. [c]$\Delta H_2 = H((THF)_4Li^+) - [H((THF)_3Li^+) + H(THF)]$. [d]$\Delta H_3 = H(SSIP) - [H(R^-) + H((THF)_4Li^+)]$. [e]$\Delta H_{IPS} = \Delta H_1 + \Delta H_2 + \Delta H_3$.

The thermodynamic cycle depicted in Figure 3 breaks ion-pair separation into three steps: (1) ionization (ΔH_1) of the C_α–Li bond to give a trisolvated lithium cation $(THF)_3Li^+$ and carbanion $\mathbf{R}^-$; (2) solvation (ΔH_2) of the trisolvated lithium cation by a fourth THF ligand; (3) ion pair recombination (ΔH_3) of the isolated tetrasolvated lithium cation and carbanion $\mathbf{R}^-$ to form the SSIP. The geometries and absolute energies of the isolated carbanions and THF-solvated lithium cations are provided in the Supporting Information.

As can be seen in Table 3, the ionization of tritylllithium $\mathbf{3_C}$ is least endothermic at +74.7 kcal/mol; the ionization of diphenylmethyllithium $\mathbf{2_C}$ and fluorenyllithium $\mathbf{1_C}$ are 6–8 kcal/mol more endothermic at +81.2 and +82.5 kcal/mol, respectively. This trend in ionization enthalpy (ΔH_1) matches the trend in observed experimental values for ΔH_{IPS}: trityl < diphenylmethyl ~ fluorenyl. Note that the order of ionization enthalpies ΔH_1 differs considerably from the order of acidity (DMSO) of the corresponding hydrocarbons. In DMSO, Fl–H is the most acidic (pK_A = 22.6),[52] reflecting aromatic stabilization gained in the carbanion; DPM–H and Tr–H are 8–10 orders of magnitude less acidic (pK_A = 32.3[52] and 30.6,[51] respectively). That fluorenyllithium $\mathbf{1_C}\cdot(THF)_3$ has the most endothermic ΔH_1 among diphenylmethyllithium $\mathbf{2_C}\cdot(THF)_3$ and tritylllithium $\mathbf{3_C}\cdot(THF)_3$ therefore suggests that steric effects play an important role in ionization of the C_α–Li bond. Bulky tritylllithium $\mathbf{3_C}\cdot(THF)_3$ would enjoy greatest loss of steric compression on ionization, and correspondingly has the least endothermic ΔH_1 value.

Next, we looked at solvation (ΔH_2) of the trisolvated lithium cation by a fourth THF molecule to form the tetrasolvated lithium cation. As expected, this process is highly exothermic with ΔH_2 being −16.3 kcal/mol at B3LYP/6-31G* in a vacuum. This value, since it is calculated without an anionic fragment, applies equally to the **1**–**3**. Lastly, we looked at the ion-pair recombination step (ΔH_3) to assess its contribution to the overall ion-pair separation process. As expected, ion-pair recombination is highly exothermic, reflecting strong ionic interaction in the SSIP (ΔH_3 = −59.5 to −64.2 kcal/mol; Table 3). The trend obtained for ΔH_3 was opposite to the trend of ΔH_1; this reversal was expected, as the two are complementary reactions. Thus, just as ionization (ΔH_1) is least endothermic for $\mathbf{3_C}$, ion-pair recombination (ΔH_3) is the least exothermic for $\mathbf{3_S}$. Finally, we note that the aforementioned trends in ΔH_1, ΔH_2, and ΔH_3 at B3LYP/6-31G* are also seen at MP2/6-31G*//B3LYP/6-31G*. As was seen for ΔH_{solv3}, the magnitudes of ΔH_1, ΔH_2, and ΔH_3 at MP2/6-31G*//B3LYP/6-31G* are considerably larger than they are at B3LYP/6-31G*. However, as Table 3 illustrates, the sum of the bond-breaking (ΔH_1), bond-making (ΔH_2), and ionic association steps (ΔH_3) gives nearly identical values of ΔH_{IPS} at both B3LYP/6-31G* and MP2/6-31G*//B3LYP/6-31G*.

Application of Solvent Continuum Models to the Ion-Pair Separation of Explicit Solvates. To this point we have attempted to match experimental enthalpies for ion-pair separation of **1**–**3** in THF solution by modeling explicit THF solvates in vacuo. These vacuum calculations match the experimental observations that IPS of tritylllithium $\mathbf{3_C}$ is more exothermic than that of diphenylmethyllithium $\mathbf{2_C}$ or fluorenyllithium $\mathbf{1_C}$. However, as noted above, B3LYP/6-31G* values of ΔH_{IPS} are 6–8 kcal/mol less endothermic than the experimental values. This discrepancy, combined with the observation of widely disparate C_α–Li distances in the X-ray (6.854 Å)[52] and calculated B3LYP/6-31G* (5.086 Å) structures of $\mathbf{3_S}\cdot(THF)_4$, suggested that vacuum modeling of SSIPs might not well reflect their solution structures and energies. It seemed likely that dielectric effects could affect the optimum C_α–Li distance in $\mathbf{3_S}\cdot(THF)_4$ and thus in large part be responsible for the difference seen between the X-ray and calculated vacuum structures.

To rule out the possibility that the discrepancy in C_α–Li distances was due to an extremely flat B3LYP/6-31G* potential surface, we performed constrained geometry optimizations on $\mathbf{3_S}\cdot(THF)_4$, increasing the C_α–Li distance in steady increments from the vacuum value of 5.086–6.8 Å, close to the value seen by X-ray crystallography (Figure 4). At B3LYP/6-31G* this 1.714 Å increase in C_α–Li distance raised the energy by nearly 8 kcal/mol; an even larger increase of 14 kcal/mol was seen with MP2/6-31G* single-point energies (Figure 4). Thus, in a vacuum the potential surface of $\mathbf{3_S}\cdot(THF)_4$ along the C_α–Li axis is *not* flat. However, application of B3LYP/6-31G* (Onsager) and B3LYP/6-31G* (PCM) single-point energies (THF, ε = 7.58) dramatically flattened the potential surface along the C_α–Li axis: increasing the distance by 1.714 Å in these cases raised the energies by only 0.4 kcal/mol (both methods). Such a flat potential surface could easily explain the C_α–Li distance of 6.854 Å seen in the X-ray structure of $\mathbf{3_S}\cdot(THF)_4$. Finally, although relative single-point energies at MP2/6-31G* (PCM) are roughly half of those at MP2/6-31G*, at a C_α–Li distance of 6.8 Å the relative energy is still 7 kcal/mol higher in energy than at the 5.086 Å structure. Thus, MP2/6-31G* (PCM) single-point energies cannot be used to rationalize the solid-state structure of $\mathbf{3_S}\cdot(THF)_4$.

Since among all the methods examined the C_α–Li distance in the X-ray structure of $\mathbf{3_S}\cdot(THF)_4$ could only be rationalized in terms of B3LYP/6-31G* (Onsager) and B3LYP/6-31G* (PCM) single-point energies, we used these methods to calculate single-point energies at the B3LYP/6-31G* vacuum geometries of $\mathbf{1_C}\cdot(THF)_3$–$\mathbf{3_C}\cdot(THF)_3$, $\mathbf{1_S}\cdot(THF)_4$–$\mathbf{3_S}\cdot(THF)_4$, and THF. Because SSIPs are more highly ionized than CIPs, it seemed likely that application of these continuum solvation models might render ΔH_{IPS} more exothermic than seen in a vacuum. Happily, this expectation was at least partially realized (Table 4).

Application of Onsager single-point energies at the vacuum geometries rendered mean ΔH_{IPS} values 3–4 kcal/mol more exothermic than the vacuum-based values (Table 4, cf. entries 3

TABLE 4. Experimental ΔH_{IPS} and Calculated ΔH_{IPS}[a] from Onsager and PCM Single-Point Calculations at B3LYP/6-31G* and B3LYP/6-31G* (Onsager) Geometries (298 K, kcal/mol)

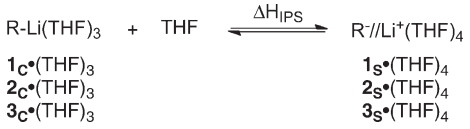

entry	method	**1** (R = Fl)	**2** (R = DPM)	**3** (R = Tr)
1	experimental	-3.8 ± 1.0[29]	-5.4 to -6.1[31]	-9.2[32]
2	B3LYP/6-31G*	+1.9	+1.9	−1.2
3	B3LYP/6-31G* (Onsager)// B3LYP/6-31G*	-1.0 ± 2.4[b]	-1.8 ± 2.6[b]	-5.5 ± 3.0[b]
4	B3LYP/6-31G* (PCM)// B3LYP/6-31G*	+1.8	+0.9	−2.1
5	B3LYP/6-31G* (Onsager)	-2.3 ± 3.4[b]	-2.8 ± 3.8[b]	-6.9 ± 4.4[b]
6	B3LYP/6-31G* (PCM)// B3LYP/6-31G* (Onsager)	+0.8	−0.3	−3.4

[a]Enthalpy value $\Delta H_{IPS} = H(SSIP) - [H(CIP) + H(THF)]$. Enthalpy corrections to absolute energies at 298 K were determined from B3LYP/6-31G* frequencies scaled by 0.9815. Experimental values determined by UV−vis spectroscopy as described in the indicated references. [b]The reported uncertainty in Onsager energy-based ΔH_{IPS} values stems from uncertainty in the radii a_0 of the spherical cavities used for the energy calculations on the CIPs, THF, and SSIPs. See the Computational Methods for complete details.

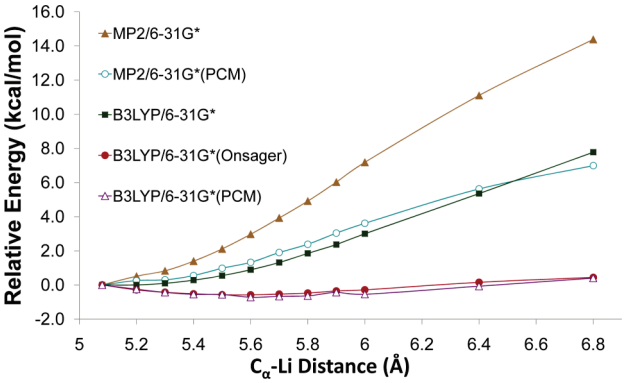

FIGURE 4. Single-point energies of B3LYP/6-31G*-constrained optimized geometries of $\mathbf{3_S}\cdot(THF)_4$ as a function of the C_α−Li distance constraint, relative to the corresponding energy at the optimized geometry (C_α−Li = 5.086 Å). Onsager and PCM single points were performed at the dielectric constant of THF (ε = 7.58).

and 2). We would stress that thermochemical calculations based on Onsager energies should generally be viewed with caution, due to uncertainty in the Onsager cavity radius a_0 (see the Computational Methods). However, based on our estimates of uncertainty, these calculated enthalpies are distinguishably more exothermic than their vacuum counterparts. With PCM single-point energies, little change was seen for the ΔH_{IPS} value of $\mathbf{1_C}\cdot(THF)_3$, but the corresponding values for $\mathbf{2_C}\cdot(THF)_3$ and $\mathbf{3_C}\cdot(THF)_3$ are 1 kcal/mol lower than the vacuum values (Table 4, cf. entries 4 and 2). These increased exothermicities prompted us to look at the effects of incorporating implicit solvation *during* the geometry optimizations.

Since B3LYP/6-31G* optimization under PCM was unsuccessful for these large explicit solvates, B3LYP/6-31G* geometry optimizations were performed with the Onsager solvation model. These Onsager-optimized geometries showed relatively minor changes for all the CIP structures, with an average 0.03 Å increase in C_α−Li bond length (see Figure S3 in the Supporting Information). In contrast, major changes were observed in the SSIP geometries, with C_α−Li contact distances increasing by 0.411−0.585 Å (Figure 5). The greatest increase in C_α−Li contact distance (0.585 Å) was seen for $\mathbf{3_S}\cdot(THF)_4$, which contains the bulkiest carbanion; the smallest increase (0.411 Å) was seen for $\mathbf{1_S}\cdot(THF)_4$, which contains the smallest carbanion. It is interesting to note that the C_α−Li distance of 5.671 Å seen in the B3LYP/6-31G* (Onsager)-optimized geometry of $\mathbf{3_S}\cdot(THF)_4$ (Figure 5) is close to the minima of the B3LYP/6-31G* (Onsager) and B3LYP/6-31G* (PCM) single-point energy curves depicted in Figure 4 (C_α−Li = 5.6 Å).

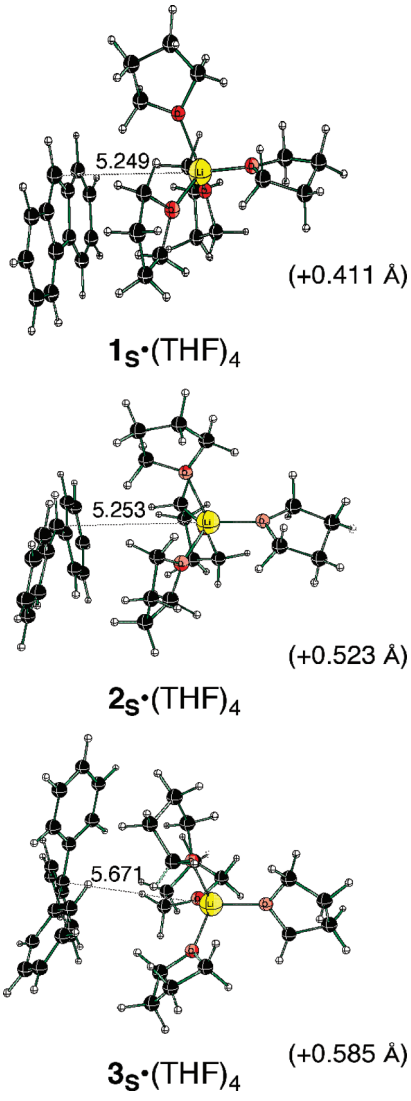

FIGURE 5. B3LYP/6-31G* (Onsager) geometries of $\mathbf{1_S}$, $\mathbf{2_S}$, and $\mathbf{3_S}$. Increases in the C_α−Li distance from the vacuum B3LYP/6-31G* geometries are given in parentheses (cf. Figure 1).

Accompanying the increases in C_α−Li distance for $\mathbf{1_S}\cdot(THF)_4$−$\mathbf{3_S}\cdot(THF)_4$ seen upon incorporating Onsager solvation during optimization, mean ΔH_{IPS} values at B3LYP/6-31G* (Onsager) are rendered 4−6 kcal/mol more exothermic than in vacuum (Table 4, cf. entries 5 and 2). PCM single-point energies at B3LYP/6-31G* (Onsager) geometries render ΔH_{IPS} values 1.1 to 2.2 kcal/mol more exothermic than in vacuum (Table 4, cf. entries 6 and 2). Looking at the values in Table 4, the apparent superiority of mean Onsager energies over PCM energies to reproduce experimental ΔH_{IPS} values (Table 4, cf. entries 5 vs 6 and 1) is intriguing, but we believe, accidental. First, the PCM cavity is more physical, corresponding much more closely to the shape of the solute than the spherical cavity used in Onsager calculations. Second, we would note that B3LYP/6-31G* (PCM)//B3LYP/6-31G* (Onsager)-based values of ΔH_{IPS} (Table 4, entry 6) in each case fall within the range of values calculated at B3LYP/6-31G* (Onsager) (Table 4, entry 5).

Conclusions

Using DFT methods, we have modeled the reaction of (THF)-solvated benzylic organolithiums **1**−**3** with THF to give the corresponding (THF)-solvated separated ion pairs (ion-pair separation). Vacuum B3LYP/6-31G* geometry optimizations gave reasonable structures for the bis(THF)- and tris(THF)-solvated contact ion pairs of **1**−**3**, and solvation free energy calculations at MP2/6-31G*//B3LYP/6-31G* indicated that the tris(THF)-solvates $\mathbf{1_C}\cdot(THF)_3$−$\mathbf{3_C}\cdot(THF)_3$ were the resting states of the contact ion pairs. Vacuum geometries of the tetrakis(THF)-solvated separated ion pairs $\mathbf{1_S}\cdot(THF)_4$−$\mathbf{3_S}\cdot(THF)_4$ were located, as were low energy ($\Delta H^{\ddagger}$ = 3.5−5.8 kcal/mol) associative transition states $\mathbf{1_T}\cdot(THF)_4$−$\mathbf{3_T}\cdot(THF)_4$ leading to these species. Calculated enthalpies of ion-pair separation (ΔH_{IPS}) for $\mathbf{1_C}\cdot(THF)_3$−$\mathbf{3_C}\cdot(THF)_3$ at B3LYP/6-31G* in vacuum ranged from +1.9 to −1.2 kcal/mol.

Application of continuum solvation models (THF, ε = 7.58) was found to have a significant affect on equilibrium B3LYP/6-31G* C_α−Li distances in the SSIPs $\mathbf{1_S}\cdot(THF)_4$−$\mathbf{3_S}\cdot(THF)_4$, as one might expect for highly ionic species (Figures 4 and 5). The X-ray crystal structure of $\mathbf{3_S}\cdot(THF)_4$ cannot be rationalized on the basis of B3LYP/6-31G* or MP2/6-31G*//B3LYP/6-31G* energies; only when implicit solvation models are included at B3LYP/6-31G* can the observed 6.856 Å C_α−Li distance[52] be understood (Figures 4 and 5). Furthermore, we have shown that application of continuum solvation models (B3LYP/6-31G* (PCM)//B3LYP/6-31G* (Onsager)) renders ΔH_{IPS} values 1.1−2.2 kcal/mol more exothermic than the corresponding vacuum values, thus bringing them closer to experiment.

We believe that the principal value of our approach lies in *qualitative* rather than quantitative agreement with experiment. The gap remaining between B3LYP/6-31G* (PCM)//B3LYP/6-31G* (Onsager) and experimental values of ΔH_{IPS} (4.6 to 5.8 kcal/mol) suggests that implicit solvation models may not be able to fully account for the role of bulk solvent. To highlight this point, preliminary calculations estimate the correction for basis set superposition error (BSSE) may further increase this gap by up to 5 kcal/mol.[61] Consideration of explicit solvent molecules outside the primary solvation shell may prove essential, suggesting that use of QM/MM/Monte Carlo[62,63] or MD[36,37] methods might be required to achieve closer agreement of calculated ΔH_{IPS} values with experiment.

Acknowledgment. We thank the National Science Foundation (0750006) and the Virginia Tech Department of Chemistry for funding. We also thank Professors Ken Wiberg (Yale), Daniel Crawford (Virginia Tech), and Diego Troya (Virginia Tech) for helpful discussions and the reviewers for insightful suggestions.

Supporting Information Available: Select bond lengths and structural drawings, detailed description of iterative geometry optimization strategy, Cartesian coordinates, and absolute energies for all calculated structures. This material is available free of charge via the Internet at http://pubs.acs.org.

(61) To estimate the magnitude of BSSE, counterpoise calculations were performed on the B3LYP/6-31G* and B3LYP/6-31G* (Onsager) geometries of $\mathbf{1_S}\cdot(THF)_4$−$\mathbf{3_S}\cdot(THF)_4$. These calculations render ΔH_{IPS} more endothermic by approximately 5 kcal/mol for all three species ($\mathbf{1_C}$−$\mathbf{3_C}$), at both vacuum and Onsager geometries. See the Supporting Information for details.

(62) Chandrasekhar, J.; Jorgensen, W. L. *J. Chem. Phys.* **1982**, *77*, 5080–5089.

(63) Acevedo, O.; Jorgensen, W. L. *J. Am. Chem. Soc.* **2006**, *128*, 6141–6146.